Penn Array Receiver

Penn Array Receiver CDR Document 1: Instrument Overview

Version: 3
Date: 8th October 03

Authors: Mark Devlin, Simon Dicker, Brian Mason

Keys:

Revision History

Ver.	Changes	Date	Author
1	Draft	26 Sep 2003	Mark Devlin
2	Substantial revisions, additions	30 Sep 2003	Brian Mason
3	Revisions	9 Oct 2003	Dicker+Mason

Contents

1 Introduction

The 100 m Green Bank Telescope (GBT) is the replacement for the 300 ft telescope which collapsed in 1988. Built at the NRAO site in Green Bank, West Virginia and protected by a radio transmitter free zone, it is the world's largest fully steerable telescope. The GBT's unusual off-axis design produces an unblocked aperture with high illumination efficiency and low side-lobes.

The primary surface of the GBT is made of 2004 panels that can be positioned within 25 μm using actuators on each of their corners. Ultimately, using a laser metrology system, these actuators will control the primary surface to better than 0.21 mm RMS at all elevation angles. At 90 GHz this corresponds to an aperture efficiency of 35%. The enormous surface area of the GBT means that even with its relatively low surface efficiency, the GBT will be one of the most sensitive 90 GHz telescopes in existence. The current status of the GBT project is described in § 3.

In early 2002, our group began a collaboration with the NRAO-Green Bank team and Harvey Moseley's group at NASA Goddard to develop a 90 GHz array receiver for the GBT. The Penn Array Receiver (PAR) will employ a 64-element array of transition-edge superconducting (TES) bolometers spaced at 0.5 fλ and fed by a lens-based cryogenic optical system. In this configuration we will have a 4×4 array of fully sampled $8''$ point spread functions (PSF) producing a fully sampled $32'' \times 32''$ array. Each PSF will have a sensitivity of $215\ \mu\mathrm{Jy\,s^{\frac{1}{2}}}$. The entire array will have a mapping speed of $54\ \mu\mathrm{Jy\,s^{\frac{1}{2}}}$. In one hour the receiver will map a $15' \times 15'$ patch of sky to 120 μJy per pixel. The receiver will be mounted at the secondary focus of the GBT on the same turret that currently houses the GBT's heterodyne receivers.

The baseline specifications for the 90 GHz array call for a "user" instrument that satisfies a variety of observing requirements ranging from observations near the zenith during the best atmospheric conditions to observations 20-30 degrees above the horizon during moderate conditions. In the next section we review some of the possible science that could be carried out with this receiver, and in § 3 the specifications for a receiver that meets these goals are given. The Penn Array itself is described in § 4. Subsequent sections describe the expected effects of the atmosphere (§ 5), pertinent qualities of the GBT (§ 6), the expected sensitivity of the Penn Array (§ 7), and instrument calibration (§ 8).

2 Science with the GBT at 90 GHz

In recent years, telescope arrays such as OVRO have reached sensitivities of $13\ \mathrm{mJy\,s^{\frac{1}{2}}}$ with angular resolutions of 2–$10''$. Large single-dish telescopes that operate at 225 GHz such as the 30 m IRAM telescope currently have sensitivities around $12\ \mathrm{mJy\,s^{\frac{1}{2}}}$ and beam sizes of $28''$. Many exciting discoveries have been made with these telescopes, e.g. submillimeter studies of highly redshifted starburst galaxies that provide a good test of our theories of galaxy formation (Steidel 1999). Within our Galaxy, observations near 90 GHz have enabled astronomers to probe star-forming regions and see stellar evolution at its earliest stages (Testi 1998).

The GBT has been designed to operate at frequencies up to 116 GHz. At 90 GHz the beam size is about $8''$. Because of its large collecting area, the GBT will have a 90 GHz sensitivity much better than current millimeter wave telescopes. The GBT can switch easily between frequencies (Lockman 1998) so multi-frequency observations of a source can be taken in a single night. Some of the possible observations that could be achieved with a 90 GHz user instrument include:

- Surveys of star forming regions
- The Sunyaev-Zel'dovich Effect
- High redshift Galaxies
- Mass loss from comets
- Trans-Neptunian objects
- Galactic plane studies

Three of these are discussed in more detail below. Since the PAR on the GBT will be a user instrument there are many more applications which could not possibly be listed here.

2.1 Circumstellar Disks and Initial Stellar Mass Functions

Few doubt that the Solar System formed out a disk of gas and dust encircling the Sun some five-billion years ago. But how common are circumstellar disks? In 1990, Beckwith *et al.* used 1.3 mm continuum observations to show that 36 out of 86 pre-main sequence stars had emission that was best explained by a circumstellar disk with a mass in the range of 0.01–1$M_{\odot}$. Even though this emission was unresolved ($\ll 11''$) and their measurements had noise levels of 5 mJy/beam, Beckwith was able to determine crude radial dependencies of density and temperature of the disks by combining their data with radio and IR observations. They also claimed to have seen evidence for particle growth via adhesion.

The PAR would detect disks of a few Jupiter masses in a few seconds thereby enabling us to answer the question of *how common are systems like our solar system?* As these sources are so bright (20–800 mJy at 1.3 mm), this project would be ideal for first-light 90 GHz observations on the GBT and could be done when weather conditions do not permit other observations. By using integration times of well under a minute (in comparison to Beckwith's 200 seconds), the GBT would be able to measure 3 mm fluxes to 0.1 mJy. Such sensitive measurements would put tighter limits on Beckwith's conclusions and would enable progress to be made on the theories of the formation of planets.

More recently, Testi and Sargent (1998) completed a survey of compact millimeter-wave sources in the Serpens core. These data help to determine the initial mass functions of stars. The observations were made with the Owens Valley Radio Observatory (OVRO) at 3 mm. They detected 32 discrete sources with flux densities above 4.0 mJy in a $5.5' \times 5.5'$ region. The beam size was $5''$ and the background noise was 0.9 mJy per pixel. These observations required 50 separate pointings of the array totaling well over 100 hours of observing time. The PAR on the GBT could cover the same region to 0.1 mJy in 0.5 hrs (albeit with slightly larger pixels). A comparison of the PAR to observations with BIMA at 3.1 millimeters is made in Figure 1. The PAR will be the perfect instrument to survey large numbers of Galactic star-forming regions.

2.2 The Sunyaev-Zel'dovich Effect

The thermal Sunyaev-Zel'dovich (SZ) effect is the inverse Compton scattering of microwave background photons to higher frequencies by the hot electrons in giant clusters of galaxies. The magnitude of the SZ effect at radio frequencies is proportional to the integrated electron density through the cluster. The cluster's X-ray flux can be used to determine the size of the cluster since the flux is proportional to the integral of the square of the electron density. By assuming that the cluster gas has a spherical distribution, the angular size of the cluster can be used to estimate the distance to the cluster. Such measurements are independent of the normal distance-scale ladder and provide an independent method of measuring cosmological parameters such as Hubble's constant, H_o, and the deceleration parameter, q_o (Hughes & Birkinshaw 1998).

Typical SZ clusters are $\sim 1'$ in size and the magnitude of the SZ effect at 90 GHz is of the order of 0.2 mK. Previous detections of the SZ effect (eg: Komatsu 1999) have been made by instruments where the beam size is comparable to or larger than the cluster's core size. The possibility of contamination from point sources and non-spherical distributions of cluster gas introduce extra uncertainties in the estimation of distances to these clusters. Since a 90 GHz array on the GBT would resolve the centers of clusters, it would greatly reduce these uncertainties as well as provide critical information on the distribution of hot gas in clusters. Figure 1 shows the footprint of the PAR on a typical galaxy cluster. Additional discrimination against foreground contamination will result from comparing 90 GHz GBT observations with lower (30–50 GHz) frequency GBT observations and with higher-frequency observations made using telescopes such as the JCMT.

The PAR on the GBT will be a powerful instrument for follow up work on SZ clusters found by instruments built for making blind surveys. Several such instruments are already in the planning stage (South Pole Telescope and the Atacama Cosmology Telescope). These instruments obtain fast mapping speeds by sacrificing resolution. The resolution of the Penn Array on the GBT, and its sensitivity at a frequency where the SZE is quite strong, will enable morphological studies of SZ-discovered clusters which will be important to understanding cluster evolution and calibrating the cluster mass scale for cosmological studies.

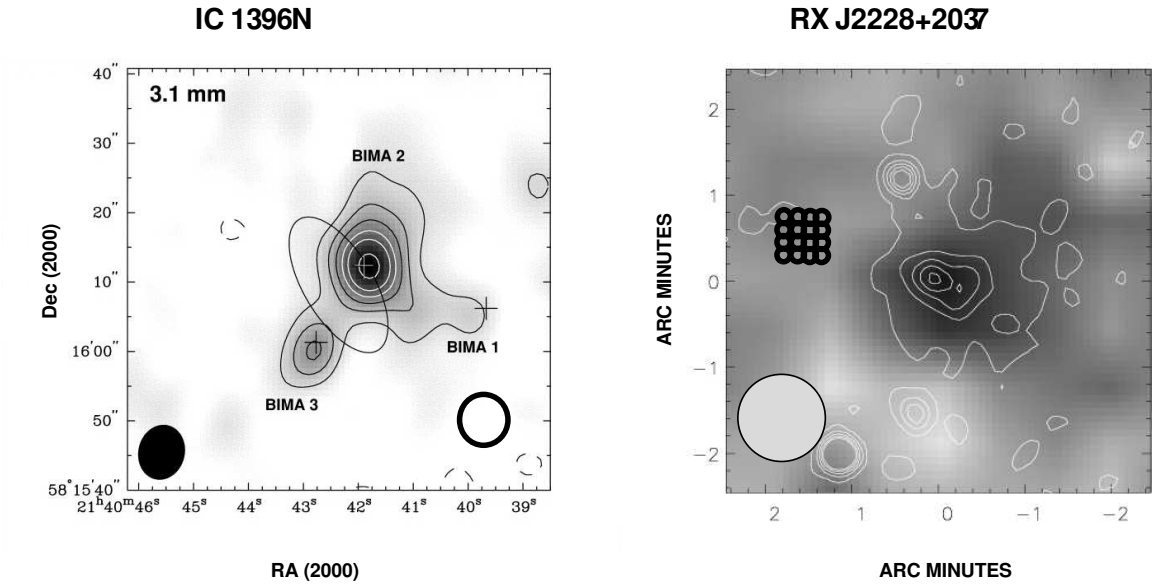

Figure 1: The GBT array will map with high resolution. Left Panel: An image of a star forming region using BIMA at 3.1 mm (from Beltran *et al.* 2002). The BIMA PSF and PAR/GBT PSF's are shown on the bottom left and right respectively. The depth of the BIMA observation (1 square arcmin) is 1.4 mJy. The PAR could map the same region to less then 100 μJy in less than 10 minutes. Right Panel: The distant galaxy cluster (SZ source) RX J228+2037 in the X-ray (contours) and at 21 GHz using the Nobeyama 45 meter telescope (from Pointecouteau *et al.* 2002) . The large circle shows the Nobeyama 80$''$ beam. The small circles show the 16 synthesized beams from the PAR. The Nobeyama measurement required 34 hours to achieve 0.05 mJy sensitivity. The PAR would require only 1 hour to achieve similar sensitivities.

2.3 High-Redshift Galaxies

At millimeter wavelengths, the flux from high ($z > 1$) redshift galaxies is enhanced due to a strong negative k-correction. The net, albeit extreme, result is that a galaxy at a redshift of 10 is 3 times brighter than the same galaxy at a redshift of 1 (Hughes 2000). In addition, when compared to observations at optical and FIR wavelengths, there are fewer problems with foreground stars and dust. Consequently, observations at millimeter/submillimeter wavelengths are a particularly attractive method for searching for high-redshift sources.

In 2001, the SCUBA camera on the JCMT completed the first 850 μm surveys covering areas of 0.002–0.12 deg^2, with 3-sigma depths in the range 1.5–8 mJy (Scott *et al.* 2002, Fox *et al.* 2002, Smail *et al.* 1997, Hughes *et al.* 1998, Lilly *et al.* 1999). Photometric redshifts will be obtained by combining the fluxes of these objects with shorter wavelength observations from future experiments such as BLAST (Devlin 2001) and with a 90 GHz survey from the GBT. Reliable redshifts have required many hours on 10 m class telescopes (or 20 hours on the IRAM PdB). These measurements are further complicated by $\sim 3''$ uncertainties in the submillimeter source positions which lead to ambiguous optical identifications. At 90 GHz, the GBT will have a resolution comparable to SCUBA's ($8''$ compared to $14''$ using SCUBA at 850 μm). Taking into account the spectrum of the submillimeter sources, the GBT will produce maps with the same signal to noise ratio as the SCUBA maps with integration times of less than a few-hundred seconds/source. Such observations would provide redshifts for many more SCUBA sources. The SCUBA surveys alone have already made a significant impact on several cosmological questions, demonstrating the usefulness of a 90 GHz GBT search for extragalactic sources.

3 Requirements of the Penn Array Receiver

With the scientific requirements in mind the following list of requirement was made. The atmospheric window at 90 GHz allows a bandpass over 18 GHz and for the greatest sensitivity the instrument will be designed for this. However excessive loading causes TES bolometer to saturate. No direct measurements of the detector loading

Receiver	Initial Receiver bandpass	8 GHz
	target Maximum Rx bandpass	18 GHz
	number of elements	64
	beam size	8”
	array geometry	8x8
	pixel spacing	$\sim 0.5 f_\lambda$
	field of view	$32''$
Detectors	Sensitivity on GBT	$247\,\mu\mathrm{Jys}^{1/2}$ ($\Delta\nu = 18\,\mathrm{GHz}$)
	(assumes 35% aperture efficiency)	$429\,\mu\mathrm{Jys}^{1/2}$ ($\Delta\nu = 8\,\mathrm{GHz}$)
	Maximum Time Constant	20 ms
	Time constant (goal)	5 ms
	$1/f$ knee	$f < 0.1\,\mathrm{Hz}$
	operable loading range	< 8 pW
Cryogenics	Detector temperature	0.3 K
	Minimum operating elevation	$< 20°$
	Maximum operating elevation	$90°$
	Duty cycle	over 90 %
	Remote operation required	
Optics	Strehl Ratio	$> 98\%$ across the array
	Spillover	$< -30\,\mathrm{dB}$
Other		Meet GB RFI requirements

Table 1: A summary of the requirements on the Penn Array Receiver.

on the GBT are possible so for the first season a bandpass of 86–94 GHz will be used. The sensitivity numbers quoted in this document are for this bandpass. The requirements on the Penn Array Receiver are summarized in Table 1.

4 The Penn Array Receiver

The GBT has two locations for receivers: the prime focus for low frequency (<1.2 MHz) receivers and a Gregorian focus where up to eight higher-frequency receivers will be installed on a rotating turret which enables the user to switch between receivers in a matter of minutes. As beam squint between orthogonal polarizations is removed at the Gregorian focus this is the chosen location for the GBT’s high frequency receivers

Currently there are plans for heterodyne receivers at the secondary focus with frequencies up to 90 GHz with dual feed horns. Operating a single pair of $8''$ pixels at 90 GHz is useful for some tests and heterodyne spectroscopy, but the state-of-the-art at these frequencies is moving rapidly towards large arrays of detectors. The PAR will be an 8×8 array of bolometric detectors that will be operated as a facility instrument.

This section describes each of the components that make up the receiver. Further details can be found in the detailed design document written for the CDR.

4.1 Detectors and Electronics

Harvey Moseley’s group at NASA-Goddard will produce the detectors for the PAR. Over the past two decades, this group has been responsible for many innovative bolometric detectors working from the X-ray to the submillimeter. Working with Kent Irwin’s group at NIST they have designed a variety of array configurations using multiplexing SQUIDs as readouts for transition-edge superconducting (TES) sensors. This type of technology is sufficiently mature that it has been chosen for the HAWC II and SCUBA II instruments. Each of these projects involves many thousands of TES detectors.

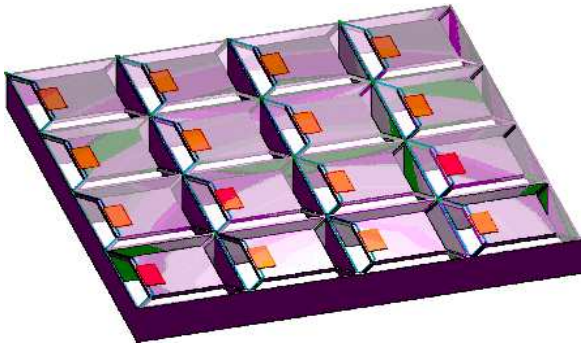

Figure 2: A 4×4 rendering of the GBT array. The 3×3 mm absorbers are each suspended by four legs. The TES for each sensor is shown in red. The final leg architecture has been tested and differs slightly from the one shown here.

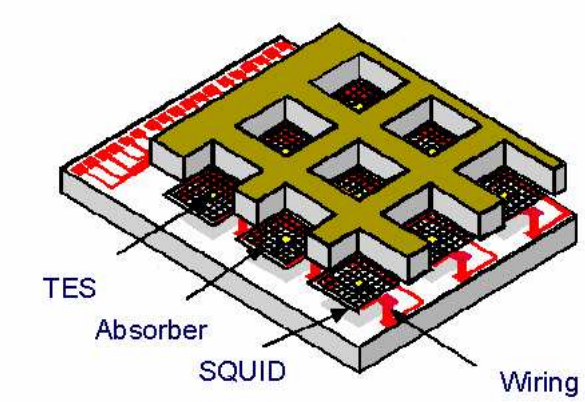

Figure 3: A cross-section of the planar array showing the major components.

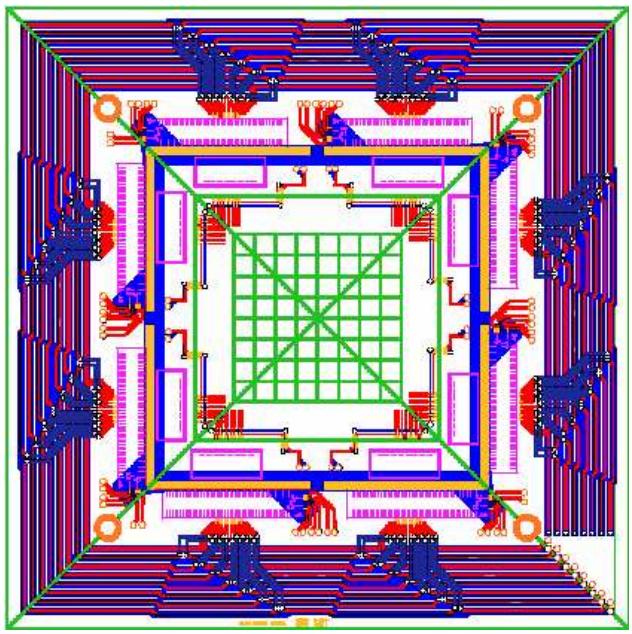

Figure 4: GBT planar multiplexed readout. In the future, a hybridized array will be the most compact detector design. The Goddard group has designed a circuit readout to demonstrate this hybrid design specifically for the GBT array. In this figure the array is the 8×8 grid in the middle with the multiplexer chips mounted around the perimeter. Figure courtesy of Benford and Wollack.

We have chosen an 8×8 planar array of bolometers without feedhorns. Figures 2, 3, and 4 show the planar architecture. These designs were made specifically for the PAR. The absorbers are 3 mm on a side and will be spaced at $0.5 f\lambda$. We plan to incorporate as much of the existing infrastructure developed for large arrays of TES bolometers as possible. This includes, digital feedback boards, cryogenic cabling, magnetic shielding, SQUIDS, and control software. While far from being "plug and play," the technology is significantly mature and modular that we can easily take advantage of the substantial efforts of these two groups. To ensure uniformity, our purchase orders for these components will be submitted in parallel with those of the Goddard group. More detailed information about similar systems can be found in Benford *et al.* 2001. However, significant progress has been made since this paper.

Many comparisons have been made between filled arrays and feed-horn coupled arrays. Griffin *et al.* 2002 note that the main advantage of filled arrays is that they provide instantaneous full sampling of the sky using $0.5 f\lambda$ pixel spacing. Griffin also points out several potential problems using filled arrays which we address here:

- The reduced integrated power per pixel for $0.5 f\lambda$ spacing may make it difficult to achieve background-limited detector performance: A ground-based array on the GBT is subject to significant atmospheric loading (see Table 2) so this will not be an issue.
- The detectors are more vulnerable to stray light and radio frequency (RF) interference because they do not have a horn to limit the acceptance angle of the absorber: The array, final lens, and Lyot stop will be kept in a cavity with T$\leq$3 K (see Figure 5). At this temperature, the total receiver load is less than 1 pW. The same cavity limits the RF. While the entrance to the cavity (the Lyot stop) is much larger than for a horn-coupled

bolometer, it is still much smaller than the expected RF wavelengths. Operating with low impedance TES detectors also reduces our sensitivity to stray RF.

- $0.5 f \lambda$ spacing requires many pixels: Multiplexing arrays make operating large numbers of detectors tractable.
- The SQUID multiplexers are sensitive to magnetic pickup: In the Goddard-NIST design, the SQUIDs are housed in a magnetically shielded box. This system has been tested and shown to provide adequate protection.

Additionally, the impedance of the TES detectors is less than an ohm, making them much less sensitive to microphonic coupling which otherwise might be a problem in the vibration-prone GBT receiver cabin. TES detectors are also insensitive to the base temperature of the receiver (a major source of 1/f noise in NTD-based bolometers).

There have been major advances in TES development over the past several years. Fabrication techniques have improved. Recently, Moseley's group has dramatically improved the noise performance of MoAu-bilayer TES bolometers. They use normal metal regions oriented transverse to the direction of current flow. Their improvements put them close to achieving the fundamental noise limits of these detectors. The results are summarized in Benford *et al.* 2003 and Staguhn *et al.* 2003.

As well as for the detectors, electronics also will monitor and control the cryogenics, measure the vacuum, and control a blackbody source which will be used as a secondary calibrator. Details of these electronics and the interface needed to operate the receiver remotely on the GBT are given in the detailed documentation for the CDR.

4.2 Cyrogenics

While bolometer development has come a long way, the ultimate sensitivity of the detector will always be a function of the base temperature of the receiver. For typical astronomical applications, an operating temperature of 300 mK is required. This low temperature can be obtained using a variety of techniques. Liquid cryogen-based cryostats require frequent transfers of cryogens which is always an inconvenience, particularly in remote locations such as the GBT receiver cabin which is 100 m above the ground. In addition, transfers would require the telescope to be parked. Another approach used on the SCUBA instrument on the JCMT is a large dilution refrigerator. Dilution refrigerators require liquid nitrogen, are large, do not provide much cooling power, and are very expensive.

A new generation of cryocooler has overcome the vibration problems associated with Gifford-McMahon (GM) systems and at the same time achieved lower base temperatures. The new cooler uses a pulse-tube technology in which an oscillating pressure (produced by a compressor located far from the cryostat) generates an oscillating gas flow in the system. Heat is removed by orifices that control the flow at the end of the cooler. This technique can obtain temperatures as low as 2.8 K and deliver 0.5 Watts of cooling at 4 K [1]. While there is still a slight amount of motion at the cold end of the tube (due to the gas flow), the vibration is much less than with standard coolers. In any case, low-impedance TES detectors are much less sensitive to any vibration than traditional high-impedance NTD-based bolometers.

We have implemented a liquid cryogen-free cooling system. It consists of two new sorption refrigerators, one using ^{4}He and one using ^{3}He. The ^{4}He refrigerator cycles directly to the pulse tube cooler. The ^{3}He refrigerator uses the cold stage of the ^{4}He as a condensation point. While there are commercial versions of these systems available, they do not provide the 15 μW of cooling at 280 mK for 3 days that our system will produce. This system is installed in a new cryostat utilizing the pulse-tube cooler. This cryogenic system is now complete. It has been fully tested under all of the observing conditions (mainly tilt angle) that it will experience as a facility instrument on the GBT. This was a major goal of the receiver project and will serve as a model for future facility instruments.

[1] A brief description can be found at `http://irtek.arc.nasa.gov/pulsetube.html`. Also see Cryomech's homepage: `http://www.cryomech.com/`).

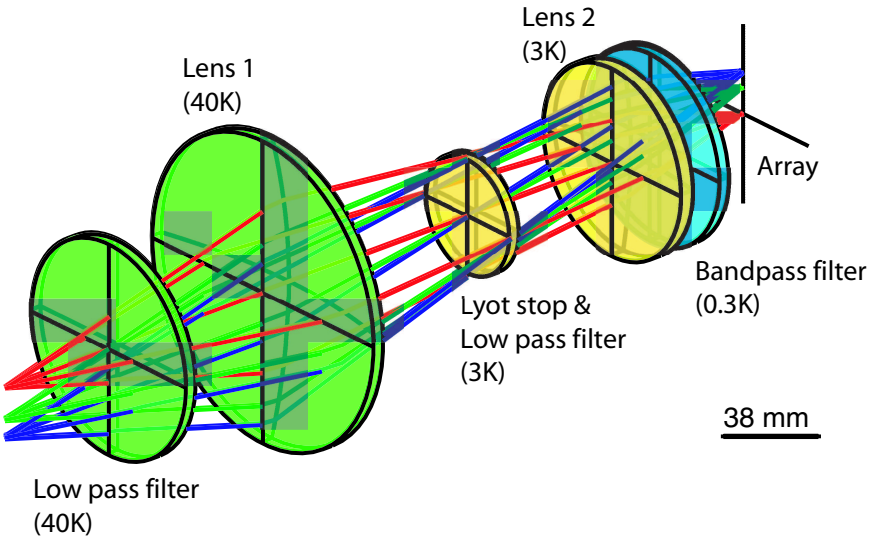

Figure 5: The position and temperature of the lenses, filters, and Lyot stop. The entire cavity containing the array, first lens, and Lyot stop is cooled to less than 3 K to reduce the thermal load on the detectors.

4.3 Cold Optics and Filters

The GBT consists of a 100 × 110 m off-axis parabolic dish with a secondary that feeds the focal plane at f/1.94. While most of the heterodyne receivers on the rotating turret use corrugated feed horns, our planar design requires us to use reimaging optics. Our design is based on several constraints:

- The detectors are spaced at $3.3\ \mathrm{mm} = 0.5\mathrm{f}\lambda$.
- The design must provide uniform performance over a 37 mm diameter focal plane.
- The illumination of the primary is determined by a cold Lyot stop placed at the primary's image.
- The array, the last lens and the Lyot stop must be kept in a cavity that has a temperature less than 3 K to reduce the load on the detectors.

We have gone through an extensive phase of optical design and review and have selected the configuration shown in Figure 5. We have taken into account the absorption and emission of the filters and lenses, the diffraction at all the apertures, and the effect of ghosting between the array and the optics. All of the parameters are well within our specifications. This design fits into a tube consisting of several modules at 300 mK, 3 K, and 40 K. The system will be assembled on the bench and inserted into the receiver.

5 The Atmosphere

At 90 GHz, the atmosphere's opacity can range from a few percent to over 50 percent, depending on location and weather conditions. Significant changes can occur on time scales of less than an hour and opacity corrections will have to be applied to all data. In addition, the atmosphere contributes a *sky temperature* signal which increases with opacity. This background will contribute to, and could even dominate, the receiver noise.

5.1 Opacity

It is possible to calculate the atmospheric opacity, τ, from the elevation, latitude, the amount of precipitable water vapor (pwv), pressure, and the well-known spectral line data of atmospheric gases (Liebe, 1985, 1989). (See

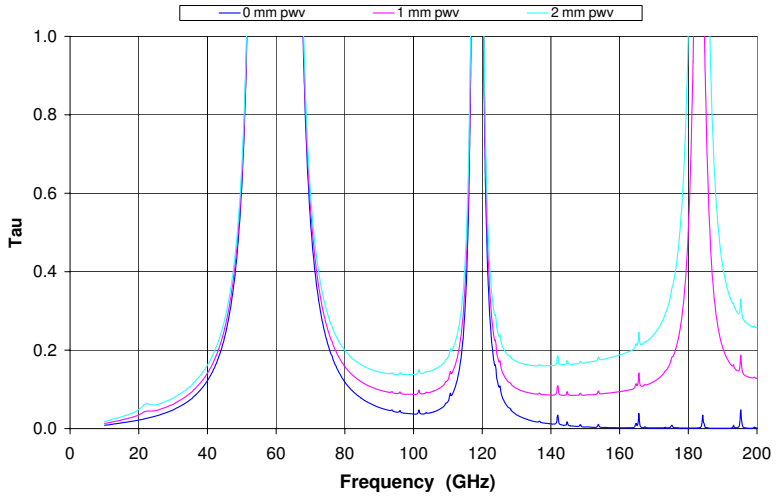

Figure 6: Calculated opacities for the atmosphere of the Green Bank site (elevation 800 m, pressure 921 mbar, temperature 286 K) using a Zhevakin-Naumov/Typo line model. In the winter we expect that the opacity will be less than 0.1 50% of the time. This corresponds to a pwv of about 1 mm.

Figure 6 for predictions for Green Bank). However these models are highly dependent on line-shape so they must be correlated with observations. NRAO has operated a 86 GHz tipper, located on the north side of the Jansky Lab, approximately 1 mile from the GBT site. Every minute, the tipper measurement of $\tau_{86\,\mathrm{GHz}}$ which all models predict is a good measure of $\tau_{90\,\mathrm{GHz}}$.

The opacity data (`http://www.gb.nrao.edu/~jbraatz/Tipper/tipper.html`), show that between December and March $\tau_{86\,\mathrm{GHz}}$ can be as low as 0.05 (a sky temperature of 15 K); in March 1999, $\tau_{86\,\mathrm{GHz}}$ was below 0.1 (a sky temperature of 28 K) for 80% of the time. The data go back to 1997. All winters show similar opacities. τ at 90 GHz is expected to be slightly lower than this value.

Although the sky temperature is large compared to the brightness temperatures of many celestial objects, much of the atmosphere will be common mode to all detectors and can be removed during data anylsis. The GBT beam is 100 m in diameter. Adjacent $8''$ beams overlap almost completely until they are outside the Earth's atmosphere. The scale height of water vapor in the atmosphere is $\approx$ 2 km, so approximately 99% of water vapor emission will be common mode over a $2'$ scan.

The exact amount of atmospheric cancellation obtained will depend on the scan strategy which is chosen for the type of observations being carried out. The simplest strategy is one of repeated drift scans. Depending on declination, the sky moves up to 2 beam widths a second. By repeatedly pointing the telescope ahead of a source and letting the rotation of the sky move the source through the beam, large amounts of sky can be covered without moving the telescope during observations and atmospheric fluctuations will be reduced. A study of scanning stratergies and the analysis software needed to use them is part of an on-going effort by NRAO staff and is reported in the software section of this design review.

5.2 Anomalous Refraction

Recent 86 GHz observations using the 14 m FCRAO telescope (Olmi 2001) have shown that anomalous refraction (AR) can move the apparent position of sources on the sky by several arcseconds on time scales of 10 to 20 seconds. The magnitude of this effect was found to be strongly correlated with the amount of water vapor in the atmosphere. With a $55''$ beam they measured average observable deflections of approximately 1.5, 1.0 and $0.5''$ when there were 4.7, 1.6 and 0.9 mm of pwv, respectively. The same effect has been observed with a similar magnitude at other very different sites (IRAM + Effelsberg).

The effects of AR on smaller telescopes is negligible due to the large beam size. The main effect of AR on the PAR's $8''$ beam will be an increase in the effecteive beam size as the quadrature sum of the average displacement

and the beam. Under the worst planned observing conditions ($\tau = 0.15$ and pwv ≈ 2 mm) we expect to increase the effective (FWHM) beam width to $\approx 8.3''$ and decrease the sensitivity by less than 10%.

6 The GBT Telescope

The current astronomical performance of the GBT has been characterized during commissioning and pointing runs at frequencies up to 43 GHz. Key aspects of antenna performance are: pointing accuracy, focus tracking, surface efficiency, and gain flatness.

The telescope pointing can be broken down into blind pointing accuracy, offset pointing accuracy, and tracking accuracy. The blind pointing accuracy measures the pointing precision after a substantial slew, and is important to allow easy acquisition of a pointing calibrator; offset pointing accuracy measures the precision after a local pointing correction has been applied by observing a nearby pointing calibration source; and the tracking error measures how accurately a given source can be tracked. The GBT's blind pointing accuracy is $\sim 10''$; since 3mm observations are expected to be obtained with periodic pointings on nearby reference sources, this is adequate performance given the Array's $32'' \times 32''$ FOV. The offset pointing accuracy has been measured at $3.2''$ (2D RMS), after the removal of a systematic source-to-source residual effect which we believe is due to correctable inadequacies in our current pointing and focus tracking models. Current *tracking* accuracy has been measured to be better than $2''$ (2D RMS). The goals for tracking and referenced pointing RMS's are each $1.3''$. K-band observations with the GBT require the telescope to be refocused every hour or so, or after a substantial slew. Focus corrections can be as large as 20mm ($\sim 25\%$ in gain at 20 GHz). The Precision Telescope Control System (PTCS) project has an active program underway to improve the pointing and focus performance. Keystones of this effort will be: the network of temperature sensors recently installed on the telescope; improvements in the Finite Element Model of the telescope, and astronomical test data.

For observations above 8 GHz it is now routine to use the active surface for observations with the GBT. Observations at 20 GHz ($\lambda = 15$ mm) and 43 GHz ($\lambda = 7$ mm) yield aperture efficiencies of $\eta_A = 0.60$ and $\eta_A = 0.35$ respectively. In comparison with the long-wavelength GBT aperture effeciency of $\eta_0 = 0.7$ (for the standard illumination taper) these are consistent with a $\Delta = 470\,\mu$m surface RMS. Here we assume uncorrelated surface errors and the Ruze relation

$$\eta_A = \eta_0 \exp\left[-(4\pi\Delta/\lambda)^2\right] \tag{1}$$

The K-band measurements also show that with the active surface on the antenna gain is flat to $\pm 5\%$ or so down to 10 degrees elevation. The PTCS project is investigating approaches to improve the surface efficiency of the GBT via traditional and out-of-focus holography, improvements to the FEM, and other means. The target is $210\,\mu$m, which corresponds to $\sim 50\%$ *surface* (35% aperture) efficiency at 90 GHz.

Overall the pointing performance of the GBT is presently adequate for on-the-fly mapping, which is expected to be the primary observing mode with the Penn Array. The focus performance and aperture efficiency are more problematic, although improvements are expected over the next 12 months.

7 Expected Sensitivities and the Dependence on Loading

The goal is to build an instrument where the noise is limited by the shot noise due to the random arrival of photons. This is called BLIP noise. The Goddard group can produce detectors with noise as low as $1 \times 10^{-17} \frac{\mathrm{W}}{\sqrt{\mathrm{Hz}}}$. This inherent detector noise is a function a variety of parameters including the operating temperature (in this case 300 mK) and the thermal conductivity, G (W/K), from the absorber to the heat sink.

For TES bolometers, the predicted loading is a critical design parameter. The thermal conductivity of the detector to the heat sink must be designed to keep the bolometer near the transition region while it is under load. If the loading gets too high, the sensor will go to a normal conducting state and not function. For balloon or space applications, determining the loading is a straightforward calculation including mostly the receiver and the optics. For a ground based instrument, we must also include a significant contribution from the atmosphere. Table 2 gives

Observing Conditions (opacity),(fraction of time)	Zenith Angle	Loading (pW) 81-99 GHz	Loading (pW) 84-96 GHz	Loading (pW) 86-94 GHz
Excellent Winter	Z = 0	1.26	0.84	0.56
($\tau \leq 0.07$),(10%)	Z = 70	3.67	2.44	1.63
Good Winter	Z = 0	1.79	1.19	0.80
($\tau \leq 0.1$),(50%)	Z = 70	5.25	3.49	2.32
Winter	Z = 0	2.69	1.79	1.19
($\tau \leq 0.15$),(70%)	Z = 70	7.87	5.24	3.49

Table 2: Atmospheric load for different observing conditions and different bands. The current design includes only the 86-94 GHz band. The fraction of observing time available for each opacity level is determined from the NRAO 3 mm tipper. They are calculated for December-March and include day and night data.

the atmospheric power at each detector for different observing conditions and observation angles. As the detectors must be designed not to saturate under the worst conditions one might wish to observe under, some sensitivity under very good conditions will be lost. Should a current proposal for funds to build a filter wheel be successful the instrument could be upgraded and the compromise between a longer observing season and better sensitivity under the best conditions can be avoided.

7.1 Mapping Speed

The sensitivity of the receiver on the GBT is determined by a combination of detector and telescope parameters. The noise of the detectors is determined by their physical parameters which are optimized for the expected loading conditions. In this case we will use a detector noise of $1 \times 10^{-17} \frac{\mathrm{W}}{\sqrt{\mathrm{Hz}}}$. For the commissioning bandpass (86–94 GHz) and atmospheric opacities greater than 0.1 the BLIP noise (dominated by atmospheric loading) is about $1.4 \times 10^{-17} \frac{\mathrm{W}}{\sqrt{\mathrm{Hz}}}$ giving a total detector noise of $n_d = 1.7 \times 10^{-17} \frac{\mathrm{W}}{\sqrt{\mathrm{Hz}}}$. The telescope response is given by:

$R = A_t \times f_t \times \epsilon_t \times a_d \times \epsilon_r \times BW \times 10^{-26} \frac{\mathrm{W}}{\mathrm{Jy}}$

Here: A_t is the area of the telescope, 8.64×10^3 m^2; f_t is the fraction of the area used by the PAR, 0.74; ϵ_t is the telescope surface efficiency at 90 GHz, 0.50; a_d is the fraction of the power from a PSF getting to each square detector with a $0.5 f\lambda$ spacing, 0.22 (Griffin *et al.* 2002); ϵ_r is the receiver efficiency, 0.5; BW is the bandwidth, 8 GHz.

For commissioning the sensitivity of each detector is then:

$S_d = n_d/R = 607 \frac{\mu\mathrm{Jy}}{\sqrt{\mathrm{Hz}}}$, or $429\ \mu\mathrm{Jy\ s}^{\frac{1}{2}}$

To fully sample the sky with $0.5 f\lambda$ detector spacing, four detectors must be combined in quadrature resulting in a total noise of $215\ \mu\mathrm{Jy\ s}^{\frac{1}{2}}$ for each of 16 fully sampled $8''$ PSFs. This gives a mapping speed for the array of $54\ \mu\mathrm{Jy\ s}^{\frac{1}{2}}$ per pixel. If our atmospheric models turn out to be accurate it will be possible to increase the bandpass to 18 GHz, increasing the mapping speed to $31\ \mu\mathrm{Jy\ s}^{\frac{1}{2}}$ per pixel. The PAR is compared to other instruments in Table 3. The sensitivity will scale roughly with the square root of the atmospheric loading given in Table 2.

To map brighter sources, the telescope could be operated in drift scan mode so that ≈ 2 beams would pass each detector every second. In drift scan mode 0.034 deg^2 could be mapped to a 1-sigma depth of 0.10 mJy every hour. This mapping strategy would remove possible errors due to drive motors exciting vibrations in the telescope structure.

8 Calibration and Beam Characterization

Absolute and relative calibration are essential components of any observing program. The nature of the bolometric receiver requires several levels of calibration on a variety of time scales. The response of the bolometers will vary

Telescope/Instrument	Type	wavelength (millimeters)	Beam	1 hr Depth 15'×15'
IRAM+MAMBO II	Bolometer	1.2	$28''$	1.7 mJy
OVRO	Heterodyne Array	3	$1.7''$- 11´	59 mJy
BIMA	Heterodyne Array	3	0.36 - $18.8''$	26 mJy
CSO+BOLOCAM	Bolometer	1.2	$40''$	1 mJy
LMT+BOLOCAM	Bolometer	1.2	$8''$	1 mJy
Nobeyama	Heterodyne	3	2 - $6''$	21 mJy
GBT+PAR	Bolometer	3	8"	**0.12 mJy**

Table 3: A comparison of the PAR to other millimeter instruments. The mapping speed is represented by the RMS noise per pixel for a $15' \times 15'$ map. For the PAR a 70% observing efficiency and 8 GHz bandpass is assumed.

due to changes in electronic gain. The response of the system will vary with the sky opacity (a function of time and zenith angle) as well as the beam efficiency of the instrument (also a function of time and zenith angle).

Absolute calibration is best carried out using observations of astronomical sources with angular sizes much less than the beam size. These sources should be bright enough to give high signal-to-noise ratios with a few seconds integration, and should have steady, well known fluxes. We will use Uranus, Mars and Neptune which have angular sizes of approximately $3''$. These planets have been used as calibrators for other observations (Beckwith 1990, Testi 1998). Large asteroids can also be used as calibrators. Since asteroids lack atmospheres, their spectral energy distributions can be modeled at longer wavelengths (Mueller *et al.* 1998, 2002). Because of their brightness and small size, asteroids will also serve to characterize the beam profile across the array.

We will use a secondary calibrator to obtain more stable calibrations between observations of astronomical sources. Several pulsed thermal sources will be placed just outside the edge of the Lyot stop. These sources (essentially fast, black bolometers) will produce a pulse before and after each absolute calibration. By activating the thermal source periodically throughout an observation, the absolute calibration will be transferred to shorter time scales. The net result is that time-consuming planetary calibrations will only have to be repeated every several hours, or because of changing observations or conditions. Because they are located at the Lyot stop, these calibration sources will also measure the flatness of the response across the array.

References

1. Beckwith, S.V.W., *et al.* 1990, AJ vol 99, 924 - 945
2. Beltran, M., *et al.* 2002, ApJ, 573, 246
3. Benford, D.J., *et al.* 2001, International Journal of Infrared and Millimeter Waves, 21:12, 1909
4. Benford, D.J., *et al.* 2003, Proceedings of the 10th International Workshop on Low Temperature Detectors
5. Devlin, M.J., 2001, Deep Millimeter Surveys, Proceedings of the UMASS/INAOE conference, 2001 Word Scientific Publishing, ISBN 9810244657. See also `http://chile1.physics.upenn.edu/blastpublic`
6. Griffin, M.J., Bock, J.J., Gear, W.K., 2002, astro-ph/0205262
7. Fox, M.J., *et al.* , 2002, MNRAS, 331:4, 839
8. Glanz, J., 1999, New York Times, 11/26/1999, Sec. A, 1
9. Komatsu E. 1999, ApJ, 516, L1
10. Hughes D. *et al.* 1998, *Nature*,394, 241
11. Hughes D. Clustering at High Redshift, ASP Conference Series, Vol. 200. Edited by A. Mazure, O. Le Fvre, and V. Le Brun. ISBN: 1-58381-027-7 (2000), p.81
12. Hughes J.P., Birkinshaw M. 1998, ApJ, 501, 1
13. Liebe H.J., 1985, Radio Sci., 20, 1069
14. Liebe H.J., 1989, Int. J. Infrared Millimeter Waves, 10, 630
15. Lilly S. *et al.* 1999, astro-ph/9901047, in press
16. Lockman J. 1998, SPIE, 3357, 656
17. Mueller, T.J., *et al.* 1998, A&A, 338, 340
18. Mueller, T.J., *et al.* 2002, A&A, 381, 324
19. Miller A.D. *et al.* 1999, ApJ vol 524, L1-4
20. Miller, A.D. *et al.* 2002, ApJS, 140, 2
21. Norrod D. 1995 GBT memo
22. Olmi, L. 2000,LMT/GMT project - private communication
23. Olmi, L. 2001 A&A 374, 348
24. Pointecouteau, E. *et al.* 2002, A&A, 387, 56
25. Puchalla, J.L., *et al.* 2002, AJ, 123, 4
26. Scott, S.E. *et al.* 2002, MNRAS 331:4, 817
27. Smail I., Ivison, & Blain A.W. 1997, MNRAS, 490, L5
28. Staugh, J., *et al.* 2003, Proceedings of the 10th International Workshop on Low Temperature Detectors
29. Steidel C.C., 1999, Proc. Natl.Acad.Sci.USA, Vol 96, 4232
30. Testi, L., Sargent, A.I., 1998, ApJ vol 508, L91-95
31. Torbet, E. *et al.* 1999, ApJ vol 521, L79-82